Composites: Part B 59 (2014) 196–203

Contents lists available at ScienceDirect

Composites: Part B

journal homepage: www.elsevier.com/locate/compositesb

# Non-destructive testing of low-energy impact in CFRP laminates and interior defects in honeycomb sandwich using scanning pulsed eddy current

Yunze He [a,b,*], GuiYun Tian [b], Mengchun Pan [a], Dixiang Chen [a]

[a] College of Mechatronics Engineering and Automation, National University of Defense Technology, Changsha 410073, PR China
[b] School of Electrical and Electronic Engineering, Newcastle University, Newcastle upon Tyne NE1 7RU, UK

ARTICLE INFO

*Article history:*
Received 14 July 2012
Received in revised form 30 October 2013
Accepted 7 December 2013
Available online 15 December 2013

*Keywords:*
A. Carbon fibres
B. Delamination
B. Impact behaviour
D. Non-destructive testing

ABSTRACT

With the growing interest to use composite materials and honeycomb sandwich panels in industrial fields, much attention is devoted to the development of non-destructive testing (NDT) techniques for the detection and evaluation of defects. In this work, scanning pulsed eddy current (PEC) was investigated and two features, representing the magnetic field intensity and conductivity, were used to characterise the different types of defects in carbon fibre reinforced plastics (CFRP) laminates and honeycomb sandwich panels. The experimental results show that the low energy impact from 4 J to 12 J, conductive and non-conductive insert defects can be effectively detected and evaluated using the proposed methods. The effectiveness was verified and the advantages of scanning PEC were addressed through comparative studies with flash thermography and shearography.



## 1. Introduction

In recent decades, there has been an increasing interest in the use of composite materials and structure, like carbon fibre reinforced plastics (CFRP) and sandwich honeycomb structure in many industrial fields, because of the low weight and improved mechanical properties compared with metals. On one hand, random porosity or undesirable material may appear in composite structures during manufacturing process. On the other hand, outside impacts may result in delamination or disbonding when structures are in service [1]. These undesirable inclusions or defects affect the structure and its mechanical properties. In order to check the integrity of the composite structures, these defects have to be detected and evaluated after manufacturing and monitored during in-service operation. To accomplish this, non-destructive testing (NDT) techniques are investigated [2–5], such as ultrasonic testing [6], X-ray [3], eddy current (EC) [7], microwave [8], electrical resistivity measurement [9], acoustic emission[10], flash thermography [11,12], and shearography [13].

Eddy current, widely used for detecting defects in metallic components, can be used in detection of conductive composite material, like CFRP [7] and metal–matrix composites [14]. EC testing offers a number of advantages compared to other NDT techniques: it enables detection of surface and subsurface damage in contrast to dye penetrant inspection; it can be applied to non-magnetic metallic items in contrast to magnetic flux leakage; it does not require an acoustic couplant as is the case for ultrasonic inspection, and it is more economical, easily applied, and less hazardous than radiography. Pulsed eddy current (PEC) technique is an important advance over other EC methods, which has been proved as an effective tool for flaw detection and corrosion detection in metals [15–17]. In previous works, various features are selected and used to represent the conductivity change by stress in aluminium [18] and permeability variation in steel corrosion [19]. In this paper, scanning PEC is applied in detection and evaluation of defects in CFRP laminates and honeycomb sandwich panels, and appropriate features are extracted to characterise the surface impact defects and inner delamination.

Over the past twenty years, optical methods have gradually appeared and are now being applied to NDT field. The major advantage of optical methods over other NDT techniques is that optical methods are able to inspect a large area in a relatively short time. Flash thermography is commonly used for metallic samples and composite material, which can reveal many defects: impact damage, delamination, disbonding, etc. Shearography derived from speckle interferometry is a new method, which is used to determine the strain field of a given specimen. Delamination, disbonding or wrinkles can be detected using this method [20]. However, these optical methods are not yet used on an industrial level because the results are relatively hard to analyse, and there is also

* Corresponding author at: College of Mechatronics Engineering and Automation, National University of Defense Technology, Changsha 410073, PR China.
*E-mail addresses:* hejicker@163.com (Y. He), g.y.tian@ncl.ac.uk (G. Tian).

1359-8368/$ - see front matter © 2013 Elsevier Ltd. All rights reserved.
http://dx.doi.org/10.1016/j.compositesb.2013.12.005

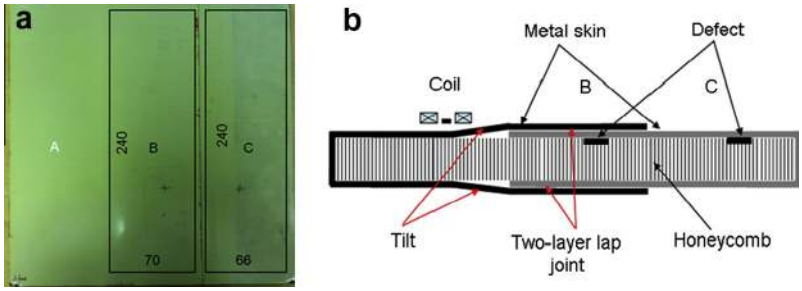


**Fig. 1.** Honeycomb sample 1: (a) top view; and (b) section view schematic.

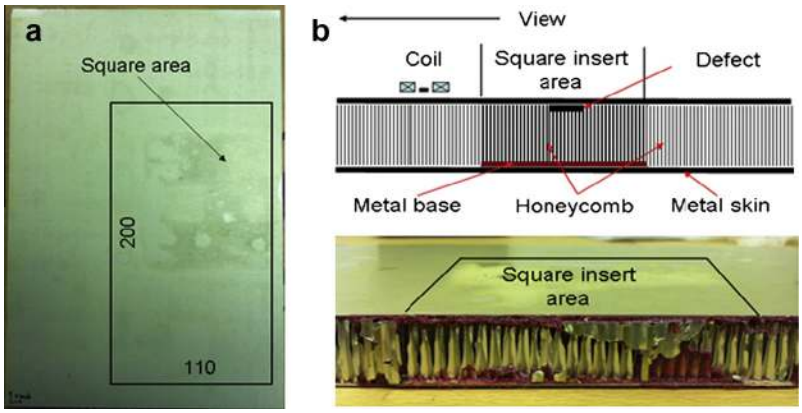


**Fig. 2.** Honeycomb sample 2: (a) the backside photo; and (b) section schematic and photo.

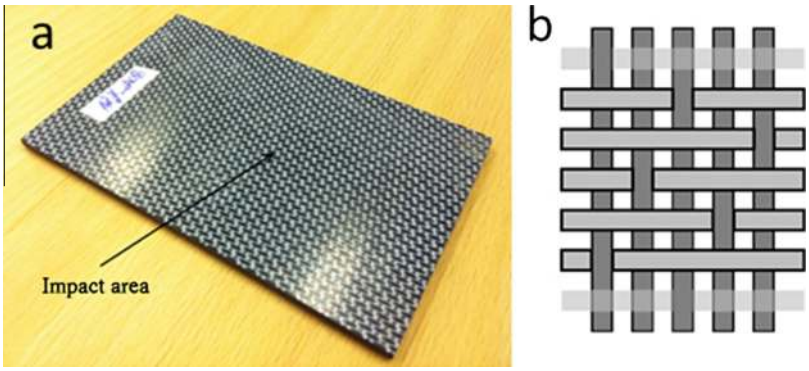


**Fig. 3.** (a) Photo of the CFRP sample; and (b) scheme of 5HS carbon fibre woven.

a lack of both standardization and operator training [1]. In this work, for comparing characteristics and verifying the effectiveness of scanning PEC, the same samples are tested using flash thermography and shearography.

The aim of the present study is firstly to inspect the various specific aeronautical specimens (sandwich honeycomb with inner defects and CFRP with impact damage). The second aim is to verify the effectiveness of applying scanning PEC to detect defects. The rest of the paper is organized as follows. Firstly, specimens are introduced in Section 2. Then, scanning PEC system and related features are introduced in Section 3, which is followed by experimental studies of defect characterisation in honeycomb sandwich panels and CRFP laminates in Section 4. Finally, the conclusions and further work are outlined in Section 5.

## 2. Specimen description

### 2.1. Honeycomb sandwich structure

Honeycomb sandwich structures are used extensively on both civil and military aircraft due to their high stiffness and low weight [21]. They also provide a material with minimal density and relative high out-of-plane compression properties and out-of-plane

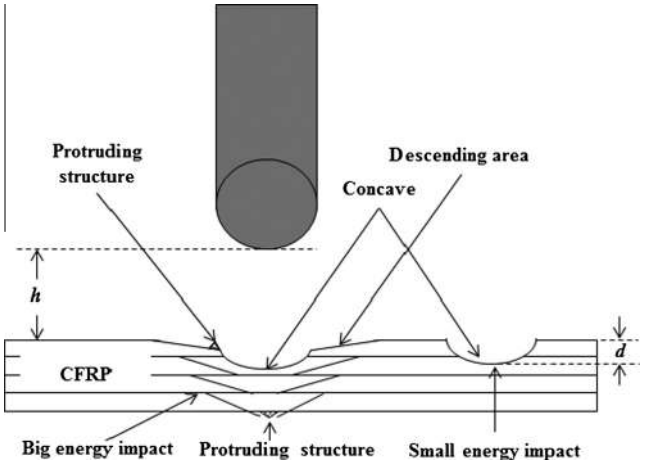


**Fig. 4.** General impact characteristics for CFRP structures.

shear properties. In the service life of a sandwich panel, impacts are caused by debris during aircraft takeoffs and landings, dropping tools during maintenance, or even collisions by birds, etc. [22]. Visual inspection may reveal little damage, but significant damage (e.g. delamination, disbonding) may occur between the impacted facesheet and the core.

In this subsection, two honeycomb sandwich panels (sample 1 and sample 2) with artificial insert defects simulating inside delamination are described. They are produced by ALSTOM Ltd., Switzerland. Fig. 1 shows the top view and section view schematic of sample 1. There are two-layer aluminium skins on the area B, but one skin on the area A and C. The metal honeycomb structure is between the skins like sandwich. There are two non-conductor insert defects between the metal skin and the honeycomb on the area B and C. These defects can affect the apparent conductivity of the specimen. Fig. 2 shows the backside and section view of sample 2. There is a square insert area, which consists of one metal base and honeycomb. There are two non-conductive insert defects under the skin in the square insert area.

### 2.2. CFRP composite with impact damage

CFRP are widely used in the aerospace and renewable energy industries, because of the low weight and improved mechanical properties compared with metals [23]. Damage caused by low-energy impacts is of primary importance to the structural integrity of composites and is also among the most difficult things to detect [24]. Impacts usually incurred through foreign object damage (dropping of a tool, stone, bird strike, etc.) are the main cause of delamination in composites and can reduce their residual strength by up to 50% [25]. Low-energy impacts often leave the top surface of the component unchanged but still produce internal deformation and matrix breakage on the back surface of the component [26]. However, only one side of the components is usually accessed in situ inspection.

In this subsection, the CFRP samples providing low-energy impacts are described. As shown in Fig. 3(a), the plate samples with the size of 100 × 150 mm$^2$ have 12 layers of 5HS carbon fibre woven shown in Fig. 3(b) with quasi-isotropic global distribution [27]. The plates are 3.78 ± 0.05 mm in average thickness, 0.5 ± 0.03 in volume ratio and 1460 kg/m$^3$ in density. The polymer matrix is made of Polyphenylene Sulphide (PPS), a thermoplastic resin system [28]. The plates are produced by TenCate Advanced Composites, Netherlands.

The impact is manufactured in the middle of the sample with different energy from 2 to 12 J. General impact characteristics for CFRP structures are illustrated in Fig. 4. According the observation of impact defects, the small energy impact can result in a concave on the surface of the specimen. The big energy impacts can lead to not only a concave, but also the descending area outside of concave, some protruding structure on the edge of concave, and the protruding spot on the bottom of sample. Fig. 5 shows the microscope pictures of front side view and rear side view of 12 J impact. Clearly, some protruding spot structures appear around the concave on the front side view but the protruding structures is in the middle of impact spot on the rear side of sample. As shown in Fig. 6 of 10, 8 and 6 J impacts, with the increase of impact energy, the protruding structure on the bottom of impact spot has a decrease and there is no protruding structure found on the bottom of samples with 2 and 4 J.

## 3. Experimental set-up

### 3.1. Scanning PEC system

Fig. 7 shows the scanning PEC set-up [18,29] and the honeycomb specimen 1. The CNC X-Y scanning machine is controlled via a PC parallel interface. The scanning range, speed, and step can be set through PC-based controlling software. The QinetiQ TRECSCAN® system is used for PEC measurements. A single period of an excitation waveform is created in MATLAB and converted to an analog voltage signal by the Analog Output (AO) subsystem of a DAQ board (NI PCI-6255). The voltage signal is converted to the excitation current using TRECSCAN. TRECSCAN operates in current excitation mode with an exponentially damped square wave of duty cycle 50%, repetition frequency of 200 Hz and time constant

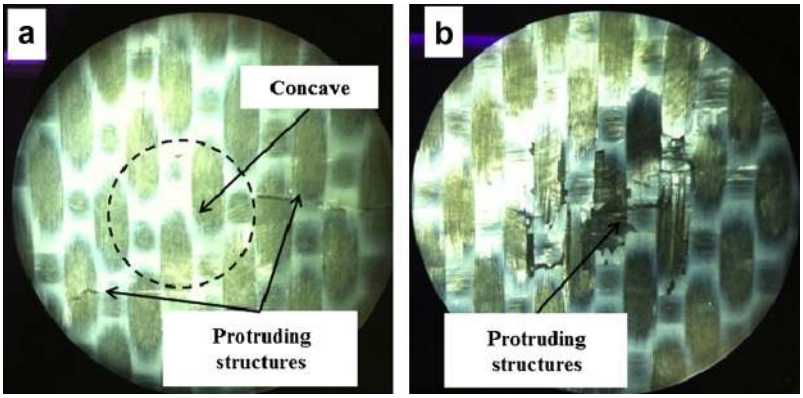


**Fig. 5.** Microscope pictures of 12 J impact: (a) front side; and (b) rear side.

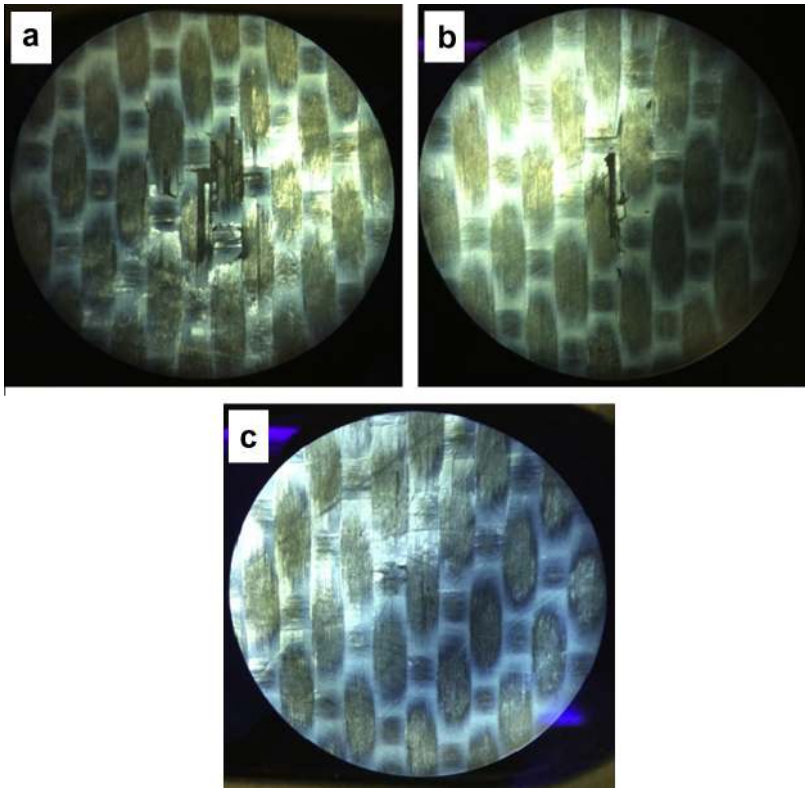


**Fig. 6.** Microscope pictures of bottom of (a) 10 J; (b) 8 J; and (c) 6 J.

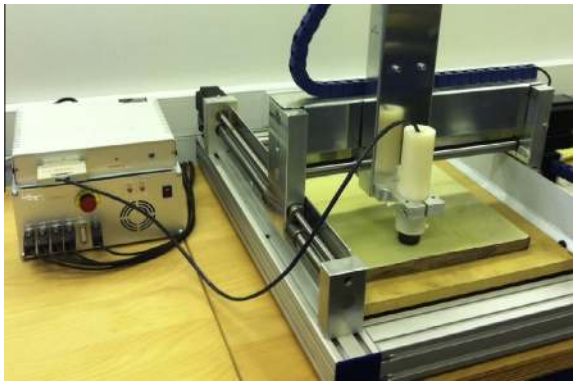

**Fig. 7.** Photograph of the scanning PEC system.

*Tc* of 100 μs. The excitation current is fed to the PEC probe. The probe consists of a ferrite core, excitation coil with mean diameter of 11 mm, and a Hall sensor. The PEC response measured by the Hall sensor is low-pass filtered (the cut-off frequency is 10 kHz) and amplified by TRECSCAN. This signal is digitised by the Analog Input (AI) subsystem of the DAQ board. The PEC response is acquired using a sampling rate of 500 kHz. The excitation wave form control, data acquisition, analysis and feature extraction are performed in MATLAB.

### 3.2. PEC feature extraction

With eddy current testing, the induction coil measures the derivative of magnetic field, while the magnetometer measures the magnetic field itself. Therefore, we select Hall sensor as the pick-up unit to map the magnetic field intensity with the help of

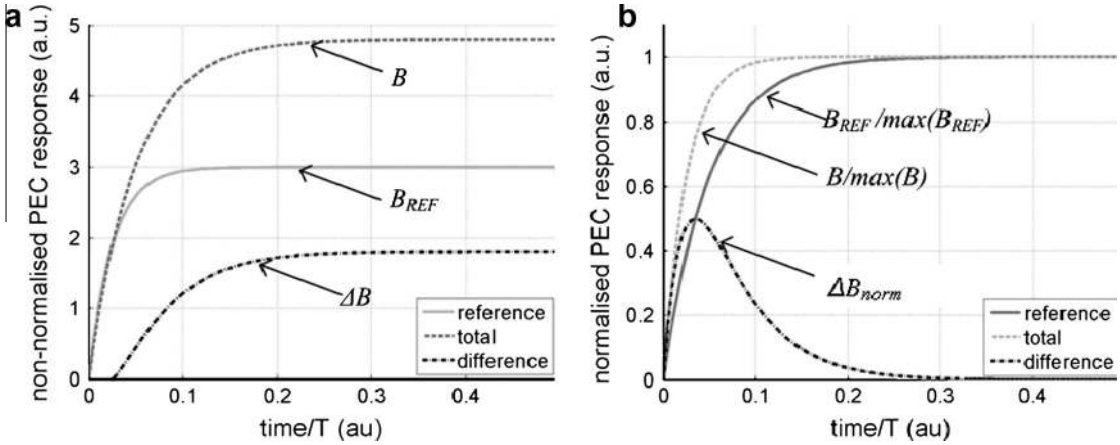


**Fig. 8.** PEC response: (a) absolute response; and (b) normalised response.

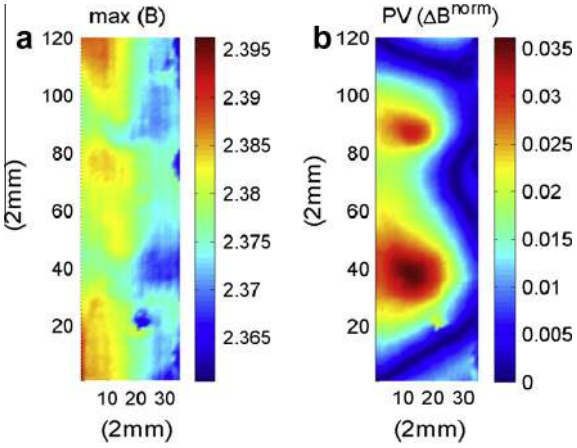


**Fig. 9.** The results of area B: (a) max($B$); and (b) $PV(\Delta B^{norm})$.

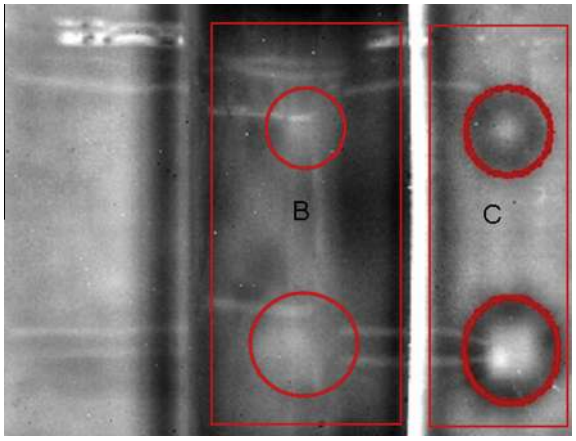


**Fig. 12.** Image of specimen 1 using flash thermography.

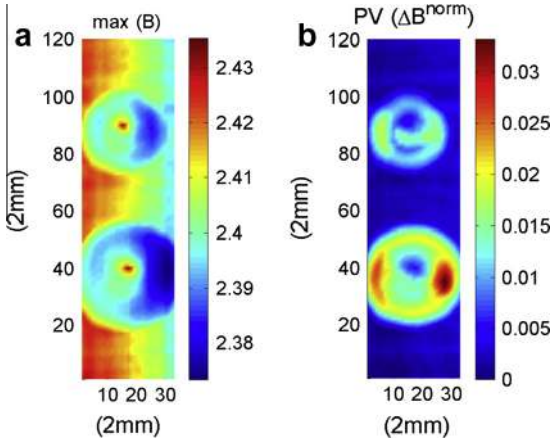


**Fig. 10.** Results of area C (a) max($B$); and (b) $PV(\Delta B^{norm})$.

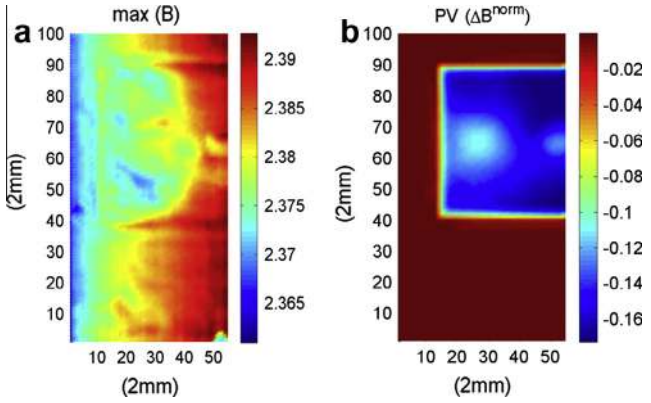


**Fig. 13.** Results of backside of honeycomb sample 2 (a) max($B$); and (b) $PV(\Delta B^{norm})$.

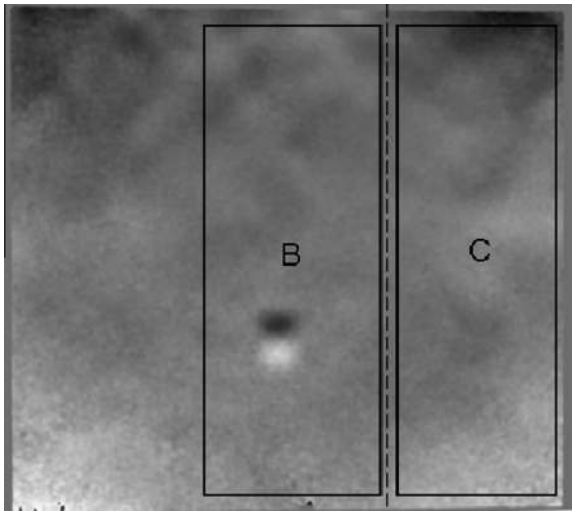


**Fig. 11.** Image of specimen 1 using shearography.

scanning set-up. The typical PEC response measured by Hall sensor in half period is shown in Fig. 8(a). The maximum of $B$ is extracted as first feature (max($B$)), which can represent the magnetic field intensity. If the material under test is a ferromagnetic material, this feature can represent the permeability of material and there is a positive monotonic relationship between max($B$) and permeability [19]. For non-magnetic material, permeability is unity and PEC response is mainly affected by conductivity, lift-off and other parameters. As shown in Fig. 8(b), another feature is $PV(\Delta B^{norm})$, the peak value of differential normalised response $\Delta B^{norm}$, which is obtained from the following equation:

$$\Delta B^{norm} = B/\max(B) - B_{REF}/max(B_{REF}) \quad (1)$$

where $B/\max(B)$ is the normalised total signal and $B_{REF}/\max(B_{REF})$ is the normalised reference signal. $PV(\Delta B^{norm})$ can represent the conductivity change of detected material, and there is a negative monotonic relationship between the feature $\Delta B^{norm}$ and conductivity [18,19]. In next work, these features are used to detect defects in honeycomb panels by mapping the conductivity distribution and to detect impacts in CFRP laminates by mapping the magnetic field intensity.

### 3.3. Other NDT methods

In order to verify the effectiveness of scanning PEC, the same samples are tested by flash thermography and shearography. The fundamental of flash thermography and shearography can be found in Section 1 and [1,30].

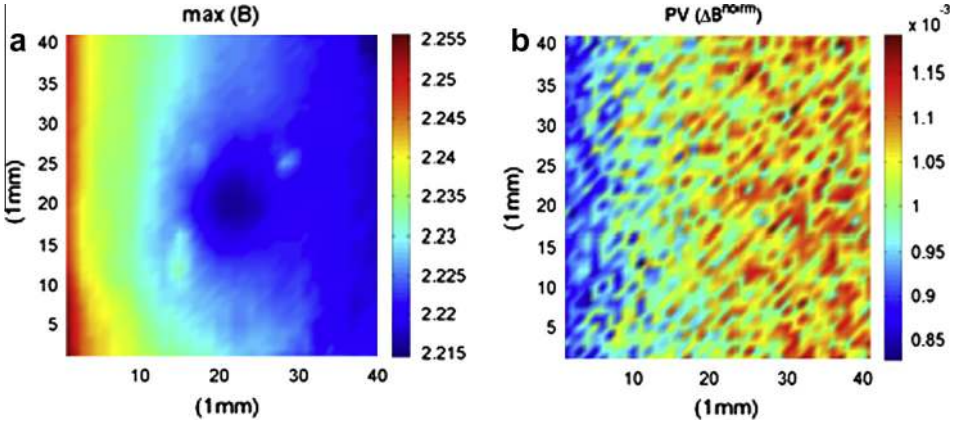


**Fig. 14.** Images of 12 J sample using (a) max($B$) and (b) $PV(\Delta B^{norm})$.

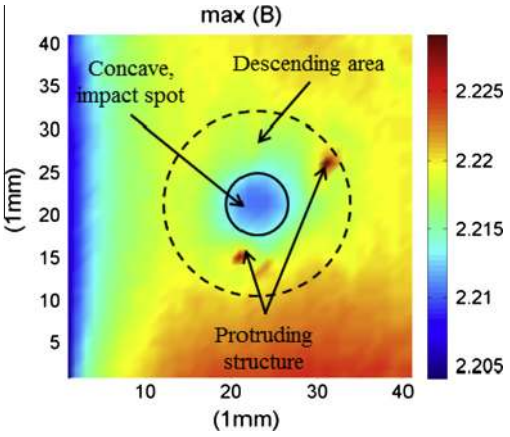


**Fig. 15.** Image of 10 J sample using max($B$).

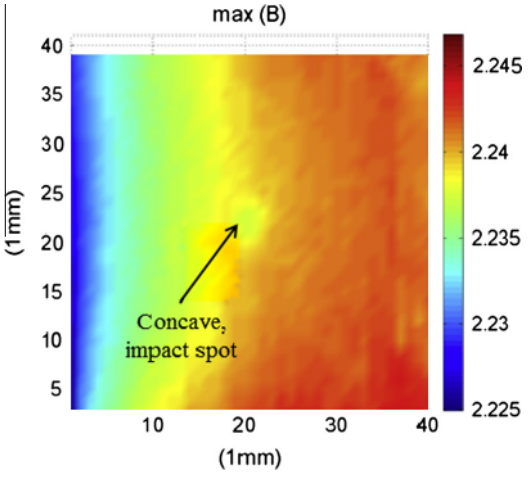


**Fig. 16.** Image using max($B$) for 4 J sample.

## 4. Experimental results

### 4.1. Honeycomb structure specimen 1

The honeycomb specimen 1 is tested using the scanning PEC system. In the experiments, the excitation frequency is 200 Hz, the sampling rate is 500 kHz and the scanning step is 2 mm. PEC probe contacts with the sample surface to reduce the lift-off effects as much as possible. The measurement for single location needs about 1.3 s and the tests for area B ($70 \times 240\ mm^2$) and C ($66 \times 240\ mm^2$) can be conducted in about 3 h. The results of area B and C are shown in Figs. 9 and 10, respectively. Clearly, there are two defects on the area B and C. As there are two-layer metal skins on the area B, the defect detectability on area B is not as good as that on area C.

Comparing two figures in Fig. 9, it is noticed that the defects in max($B$) image (Fig. 9(a)) is not as clear as $PV(\Delta B^{norm})$ image (Fig. 9(b)). This observation is in agreement with the conclusion in Section 3.2 that $PV(\Delta B^{norm})$ can represent the conductivity change of detected material. Thus, the conductivity change by defects can be shown to be more remarkable in $PV(\Delta B^{norm})$ than that in max($B$). The same phenomenon can be found in the results of area C, shown in Fig. 10. Clearly, there are two annular defects on the area C and the detectability of defects in $PV(\Delta B^{norm})$ is better than that in max($B$). The value of $PV(\Delta B^{norm})$ in the defect area shows an increase, which means that the conductivity is smaller than the defect-free area, because the defects are non-conductive.

Fig. 11 shows the result of honeycomb sandwich specimen 1 using Dantec Q-800 laser shearography system. The test can be done very quickly (around 3 min). However, just one defect in area B can be found in one test. Therefore, we can conclude that scanning PEC has the greater reliability and probability of detection (POD) for inside insert defects in honeycomb sandwich panel. Fig. 12 shows the result of specimen 1 using flash thermography. The test can also be done very quickly (around several minutes) and four defects in areas B and C can be found in one test. The flash thermography result is consistent with PEC results, which verifies the effectiveness of PEC. Although scanning PEC (about 3 h) is more time-consuming than both shearography and flash thermography, PEC has some advantages over both: (i) the PEC features can represent the physical properties of defect (conductivity); (ii) the defect visibility of scanning PEC is the best in three methods; and (iii) PEC has the greater reliability and better detectability for interior defects. These merits illustrate that scanning PEC is the right solution for aluminium honeycomb sandwich panels.

### 4.2. Honeycomb structure specimen 2

The honeycomb sandwich specimen 2 was also tested by scanning PEC. The results of rectangular area marked using black line in Fig. 2 ($110 \times 200\ mm^2$) are shown in Fig. 13. As we expected, the square area and defect area in Fig. 13(a) are not as visible as they

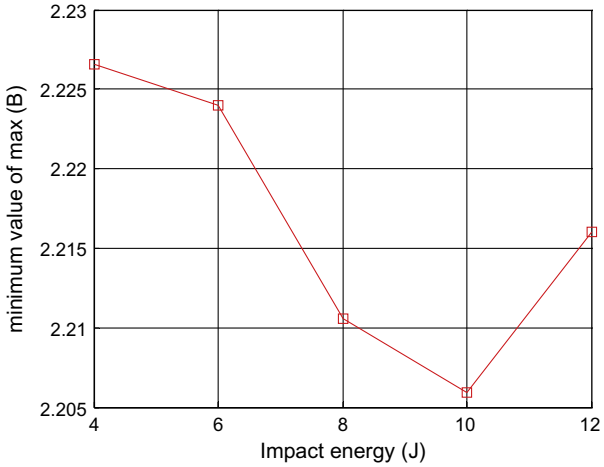


**Fig. 17.** Minimum of max($B$) on dependence of impact energy.

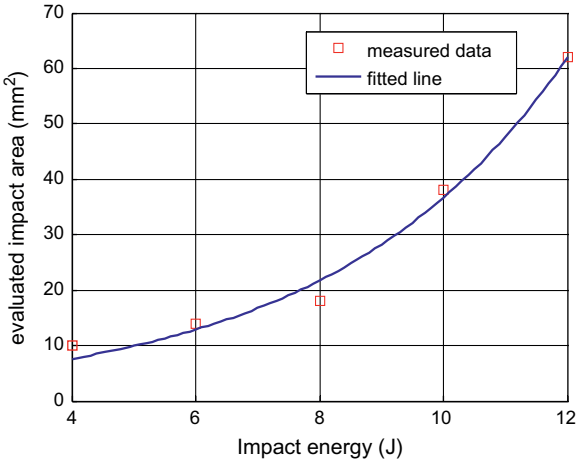


**Fig. 19.** The evaluated area against the impact energy.

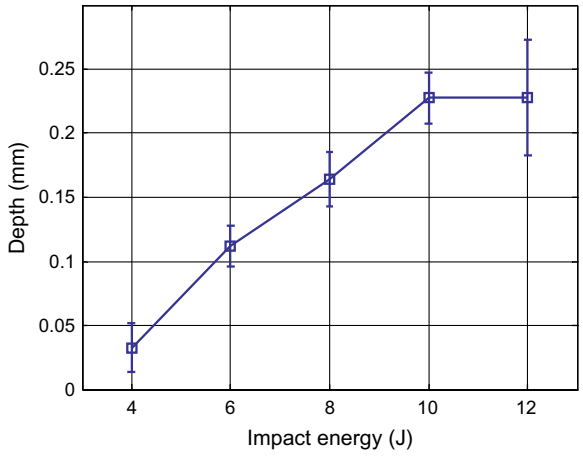


**Fig. 18.** Concave depth on dependence of impact energy.

are in Fig. 13(b). Clearly, there are one square area (blue)[1] and two circular defects in the result of $PV(\Delta B^{norm})$ in Fig. 13(b). The value of $PV(\Delta B^{norm})$ in the square area shows a great decrease over the defect-free area (red), because the square area including a metal base and honeycomb core can increase the conductivity. On the contrary, the defect areas show a bigger value in $PV(\Delta B^{norm})$ than the square area, because the defects are non-conductive and can lead to an increase in $PV(\Delta B^{norm})$. These results illustrate again that scanning PEC feature can represent the physical properties of a defect.

Usually, delamination or disbonding can occur between the metal skin and the honeycomb core during the manufacture process and throughout the service life of components. These defects can be seen as the non-conductive inserts and result in the reduced conductivity. Consequently, there will be an increased change (light spot) on the scanning PEC images of feature $PV(\Delta B^{norm})$.

### 4.3. CFRP composite with impact damage

In the scanning PEC tests of CFRP laminates, the scan area is $40 \times 40\ mm^2$ and the scan step is 1 mm. The tests can be completed in about 35 min. Fig. 14 shows the images of 12 J sample using max($B$) and $PV(\Delta B^{norm})$, respectively. Obviously, the impact can be seen in the central zone of images of max($B$) but not in the images of $PV(\Delta B^{norm})$. And, the structure of carbon woven can be more clearly observed from the images of $PV(\Delta B^{norm})$ than that of max($B$). Specifically, the impact area exhibits a decrease on the value of max($B$), which means that magnetic field intensity has a decrease due to the damage caused by impact. In addition, the descending area and some protruding structures can be found outside of the impact spot. The similar situations can be found in images of 10 J sample, shown in Fig. 15. That is because the large energy impacts can break the woven structures leading to some discontinuity on the surface. Fig. 16 shows the images of 4 J sample using max($B$). As expected, the observed impacted area is smaller than that of 10 J and 12 J because of the lower impact energy. Unlike the 10 J and 12 J, there is no descending area and disturbing spots outside impact area, because the 4 J impact is not enough to break the woven structures. According to the scanning PEC results, the 2 J impact does not lead to concave and the broken structures. Thus, the following analysis between impact energy and the PEC features is focused from 4 J to 12 J.

Fig. 17 shows the minimum value of max($B$) on dependence of impact energy. As energy increases from 4 J to 10 J, the max($B$) shows a monotonic decrease, which means that the magnetic field intensity has an decrease. However, the 12 J impact show a increase on the max($B$). The depth of the concave measured by a vernier calliper is shown in Fig. 18. From 4 J to 10 J, the depth has a continuous increase, while there is an unusual distribution for 12 J impact. The potential reason is 12 J impact leads to more structure broken (like inner delamination) than the concave.

Fig. 19 shows the evaluated area against the impact energy $W$. The blue solid line is the fitted line using an exponential function as shown in the following equation:

$$A = k_1 \exp(k_2 W) \tag{2}$$

where $W$ is the impact energy and $A$ is the evaluated area. The result illustrates that as the energy increasing, the impact has an increasing broke rate for CRFP laminates. The more appropriate relationship between impact energy and damage (concave or delamination) leaded by impact should be validated and calibrated through other NDT methods. Grimberg et al. [31] reported that the delamination has been induced by impacts with energies tap to 4 J and a linear relationship has been obtained between the area of delaminated surface and the impact energy. Our results indicate the relationship between damage and impact energy is nonlinear and the exponential function is another potential solution for impact energy predicting and analysis.

[1] For interpretation of color in Fig. 13, the reader is referred to the web version of this article.

## 5. Conclusions

In this work, scanning PEC was investigated and two features were proposed to characterise the low-energy impacts in CFRP laminates and internal inserted defects in honeycomb sandwich panels. The experimental results through scanning PEC and other optical NDT methods show that:

- The low-energy impact from 4 J to 12 J can induce the concave and other damage on the CFRP laminates. The damages can be effectively characterised using scanning PEC and the feature representing the magnetic field intensity variation. As energy increases, the impact has an increasingly broke rate on the CFRP laminates.
- The delamination in aluminium honeycomb sandwich panels affect the local conductivity and then can be effectively characterised using scanning PEC and the feature representing the conductivity variation.
- Although much more time-consuming than optical NDT methods such as flash thermography and shearography, scanning PEC has some merits: higher reliability, better defect detectability for deep defect.

The future work includes the feature extraction from PEC response measured by high sensitivity magnetic sensor based on MEMS [32,33].

## Acknowledgments

The work was supported by the EPSRC Grants EP/E005071, UK, Scholarship Award for Excellent Doctoral Student granted by Ministry of Education, China (No.: JY20101). The authors would like to thank ALSTOM® for providing the experimental honeycomb sandwich panels and flash thermography results, Prof. Grimberg in National Institute of Research and Development for Technical Physics, ROMANIA for providing the experimental CFRP samples, and Dantec® for providing the shearography tests. The authors are also grateful to China Scholarship Council for sponsoring Mr. Yunze He's visiting study to Newcastle University, UK.

## References

[1] Garnier C, Pastor M-L, Eyma F, Lorrain B. The detection of aeronautical defects in situ on composite structures using non destructive testing. Compos Struct 2011;93(5):1328–36.
[2] Zhang ZY, Richardson MOW. Visualisation of barely visible impact damage in polymer matrix composites using an optical deformation and strain measurement system (ODSMS). Compos A Appl Sci Manuf 2005;36(8):1073–8.
[3] Amenabar I, Mendikute A, López-Arraiza A, Lizaranzu M, Aurrekoetxea J. Comparison and analysis of non-destructive testing techniques suitable for delamination inspection in wind turbine blades. Compos B Eng 2011;42(5):1298–305.
[4] Ayorinde E, Gibson R, Kulkarni S, Deng F, Mahfuz H, Islam S, et al. Reliable low-cost NDE of composite marine sandwich structures. Compos B Eng 2008;39(1):226–41.
[5] He Y, Tian GY, Pan M, Chen D. Impact evaluation in carbon fiber reinforced plastic (CFRP) laminates using eddy current pulsed thermography. Compos Struct 2014;109:1–7.
[6] Hosten B, Castaings M. Comments on the ultrasonic estimation of the viscoelastic properties of anisotropic materials. Compos A Appl Sci Manuf 2008;39(6):1054–8.
[7] Mook G, Lange R, Koeser O. Non-destructive characterisation of carbon-fibre-reinforced plastics by means of eddy-currents. Compos Sci Technol 2001;61(6):865–73.
[8] Bin Sediq AS, Qaddoumi N. Near-field microwave image formation of defective composites utilizing open-ended waveguides with arbitrary cross sections. Compos Struct 2005;71(3–4):343–8.
[9] Park J-M, Lee S-I, DeVries KL. Nondestructive sensing evaluation of surface modified single-carbon fiber reinforced epoxy composites by electrical resistivity measurement. Compos B Eng 2006;37(7–8):612–26.
[10] Park J-M, Kim P-G, Jang J-H, Wang Z, Kim J-W, Lee W-I, et al. Self-sensing and dispersive evaluation of single carbon fiber/carbon nanotube (CNT)-epoxy composites using electro-micromechanical technique and nondestructive acoustic emission. Compos B Eng 2008;39(7–8):1170–82.
[11] Schroeder JA, Ahmed T, Chaudhry B, Shepard S. Non-destructive testing of structural composites and adhesively bonded composite joints: pulsed thermography. Compos A Appl Sci Manuf 2002;33(11):1511–7.
[12] Lyle KH, Fasanella EL. Permanent set of the space shuttle thermal protection system reinforced carbon–carbon material. Compos A Appl Sci Manuf 2009;40(6–7):702–8.
[13] Hung YY. Applications of digital shearography for testing of composite structures. Compos B Eng 1999;30(7):765–73.
[14] Jeong H, Hsu DK, Liaw PK. Anisotropic conductivities of multiphase particulate metal–matrix composites. Compos Sci Technol 1998;58(1):65–76.
[15] Lebrun B, Jayet Y, Baboux J-C. Pulsed eddy current signal analysis: application to the experimental detection and characterization of deep flaws in highly conductive materials. NDT E Int. 1997;30(3):163–70.
[16] Smith RA, Hugo GR. Transient eddy current NDE for ageing aircraft – capabilities and limitations. Insight: Non-Destructive Test Condition Monit 2001;43(1):14–25.
[17] He Y, Pan M, Luo F, Tian GY. Reduction of lift-off effects in pulsed eddy current for defect classification. IEEE Trans Magn 2011;47(12):4753–60.
[18] Morozov M, Tian G, Withers PJ. The pulsed eddy current response to applied loading of various aluminium alloys. NDT E Int 2010;43(6):493–500.
[19] He Y, Tian GY, Zhang H, Alamin M, Simm A, Jackson P. Steel corrosion characterisation using pulsed eddy current systems. IEEE Sens J 2012;12(6):2113–20.
[20] Hung YY. Applications of digital shearography for testing of composite structure. Compos Parts B Eng 1999;30(7):765–73.
[21] Charon A, Vodicka R, Radtke T, Chester R, Baker A. Novel technique for the evaluation of aircraft honeycomb sandwich structures. Exp Tech 2001;25(5):23–6.
[22] Foo CC, Seah LK, Chai GB. Low-velocity impact failure of aluminium honeycomb sandwich panels. Compos Struct 2008;85(1):20–8.
[23] Cheng L, Tian GY. Surface crack detection for carbon fibre reinforced plastic (CFRP) materials using pulsed eddy current thermography. IEEE Sens J 2011;11(12):3261–8.
[24] Lepine BA, Holt RT. An eddy current scanning method for the detection of corrosion under fasteners in thick skin aircraft structures. Can Aeronautics Space J 1997;43(1):28–33.
[25] Buynak CF, Moran TJ, Donaldson S. Characterization of impact damage in composites. SAMPE J 1988;24(2):35–9.
[26] Yigit SA, Christoforou AP. On the impact between a rigid sphere and a thin composite laminate supported by a rigid substrate. Compos Struct 1995;30(2):169–77.
[27] Akkerman R. Laminate mechanics for balanced woven fabrics. Compos Parts B Eng 2006;37:108–16.
[28] Grimberg R, Savin A, Steigmann R, Serghiac B, Bruma A. Electromagnetic non-destructive evaluation using metamaterials. Insight: Non-Destructive Test Condition Monit 2011;53(3):132–7.
[29] Morozov M, Tian GY, Edgar D. Comparison of PEC and SFEC NDE techniques. Nondestructive Test Eval 2009;24(1–2):153–64.
[30] Tashan J, Al-mahaidi R. Investigation of the parameters that influence the accuracy of bond defect detection in CFRP bonded specimens using IR thermography. Compos Struct 2012;94(2):519–31.
[31] Grimberg R, Savin A, Steigmann R, Premel D. Eddy current evaluation of delamination in carbon-epoxy composite materials. Bulgarian J Phys 2000;27(4):105–8.
[32] Hu J, Pan M, Tian W, Chen D, Zhao J, Luo F. $1/f$ Noise suppression of giant magnetoresistive sensors with vertical motion flux modulation. Appl Phys Lett 2012;100(24):244102.
[33] Pan H, Chen D, Pan M, Luo S, Zhang Q, Luo F. Nonlinear temperature compensation of fluxgate magnetometers with a least-squares support vector machine. Meas Sci Technol 2012;23:025008.